Influence of Land Cover and Soil Moisture based Brown Ocean Effect on an Extreme Rainfall Event from a Louisiana Gulf Coast Tropical System

Udaysankar S. Nair[1*], Eric Rappin[2], Emily Foshee[1], Warren Smith[3,4], Roger A. Pielke Sr.[4], Rezaul Mahmood[5], Jonathan L. Case[6], Clay B. Blankenship[7], Marshall Shepherd[8], Joseph A. Santanello[9], Dev Niyogi[10]

[1]Department of Atmospheric Science, University of Alabama in Huntsville, Huntsville, AL 35806

[2] Department of Geography and Geology and Kentucky Climate Center, Western Kentucky University, Bowling Green, KY 42101

[3]Department of Atmospheric and Oceanic Sciences, University of Colorado Boulder, Boulder, CO 80309

[4]Cooperative Institute for Research in Environmental Sciences, University of Colorado Boulder, Boulder, CO 80309

[5]High Plains Regional Climate Center, School of Natural Resources, University of Nebraska-Lincoln, Lincoln, NE 68583

[6]ENSCO, Inc./NASA Short-term Prediction Research and Transition (SPoRT) Center

[7] Universities Space Research Association, NASA Short-term Prediction Research and Transition (SPoRT) Center

[8]University of Georgia, Department of Geography, Atmospheric Sciences Program

[9]NASA-GSFC, Hydrological Sciences Laboratory, Greenbelt, MD

[10]Department of Agronomy and Department of Earth, Atmospheric and Planetary Sciences, Purdue University, West Lafayette, IN 47907, USA

[*] Correspondence to nair@nsstc.uah.edu

Submitted to Scientific Reports

First Revision: August 15, 2019, 2nd Revised Submission: September 2019

ABSTRACT

Extreme flooding over southern Louisiana in mid-August of 2016 resulted from an unusual tropical low that formed and intensified over land. We used numerical experiments to highlight the role of 'Brown Ocean' effect (where saturated soils function similar to a warm ocean surface) on intensification and it's modulation by land cover change. A numerical modeling experiment that successfully captured the flood event (control) was modified to alter moisture availability by converting wetlands to open water, wet croplands, and dry croplands. Storm evolution in the control experiment with wet antecedent soils most resembles tropical lows that form and intensify over oceans. Irrespective of soil moisture conditions, conversion of wetlands to croplands reduced storm intensity, and also, non-saturated soils reduced rain by 20% and caused shorter durations of high intensity wind conditions. Developing agricultural croplands and more so restoring wetlands and not converting them into open water can impede intensification of tropical systems that affect the area.

INTRODUCTION

A tropical disturbance formed over the southern part of Louisiana in mid-August 2016 which interacted with an eastward-moving upper-level baroclinic trough, leading to the intensification of the system and a major flood disaster [1]. This system appeared to have all of the characteristics of a tropical depression, as seen in satellite imagery and in the wind field (Figure 1a, b). Weak steering level winds, coupled with moisture, high convective available potential energy (CAPE) and a low convective inhibition (CIN) environment led to a relatively stationary system which caused local, intense rainfall over the region for several hours. Storm total accumulations from

this system exceeded 780 mm (~ 5 times the long term average rainfalls of 148 mm for Baton Rouge for the entire month of August) in the southern Louisiana, and early estimates suggest economic losses of about $8.7 billion [2]. Typically, storms such as these are remnants of decaying tropical systems that form over the ocean and propagate onshore. In this respect, this event was unusual since the tropical depression developed and persisted over land.

Conceptually, tropical cyclones (including depressions) can be viewed as heat engines powered by surface enthalpy fluxes [3]. For the heat engine to function, heat must be extracted from a large moist enthalpy reservoir (e.g., the ocean surface) and release heat, after adiabatic expansion, to a low moist enthalpy reservoir (e.g., the upper troposphere and lower stratosphere). As air spirals inward toward the center of low pressure, it undergoes near isothermal expansion, gaining moist enthalpy from the underlying surface. In other words, intensification is a function of the thermodynamic disequilibrium between the surface and the overlying near-surface atmosphere. Over the ocean, this heating is supplied by enthalpy fluxes from warm surface water, and air spirals inward isothermally. Also, warm surface water also provides an extensive source of water vapor which is essential for maintaining the strong convection in the region of lowest surface pressure. Even in the absence of significant wind shear, tropical cyclones generally decay as they migrate overland (or colder water). This is in response to a reduction in both heat input required to counteract adiabatic cooling and loss of the moisture supply or moist enthalpy for fueling deep convection [4].

The "Brown Ocean Effect"

Occasionally, a "Brown Ocean effect" can contribute to the intensification of tropical cyclones over land [5–9]. The Brown Ocean effect refers to saturated soils, swamps and wetlands in the inland

regions providing a source of moist enthalpy for maintaining tropical cyclone warm-core structures and inland intensification [6,8,10]. Thus, realistic representation of surface enthalpy fluxes is important for accurate model predictions of tropical disturbances over land [11].

Several prior modeling and observational studies attest to the role of the Brown Ocean effect contributing to the unexpected intensification of tropical cyclones over land [5,6,8,12–15]. Wetter soil conditions are found to favor formation of mesoscale convection along with land-falling systems in coastal regions [16,17]. Tropical cyclones moving inland over northern Australia are occasionally observed to reintensify through process pathways other than classical extratropical rejuvenation [5,18]. These storms retain their warm-core structure, often redeveloping such features as eyes and it is hypothesized that the revival is made possible by large vertical heat fluxes from a deep layer of very hot, sandy soil [13]. Increases in thermal diffusivity due to sandy soil wetted by the first rains from the approaching systems enable rapid upward diffusion of heat through the soil column, which is required to sustain warm-core storms of marginal hurricane intensity [10]. This intensification process is not unique to Australia; recent studies suggest that antecedent wet soils in the Indian monsoon region [16,19], as well as the southeastern US and the US Southern Great Plains, have helped create an atmosphere conducive to tropical cyclone maintenance post-landfall, by enhancing surface latent heat fluxes [15,20].

Over southern Louisiana, the moist landscape and Brown Ocean-like conditions pre-existed ith swamps, wetlands and saturated soils; we hypothesize that the above discussed tropical storm sustenance conditions occurred in southern Louisiana and contributed to the intensification of flooding during the August 2016 event. This hypothesis is tested using numerical modeling experiments to assess the role of the Brown Ocean effect, namely that the land surface functions as a reservoir of moist enthalpy, which contributed to the development of the tropical disturbance

into a persistent depression and very heavy rain over Louisiana during the period of 11-16 August 2016. Since it was located in the southern parts of Louisiana, advection of warm, moist air from the south (Gulf of Mexico) further contributed to the sustenance of the system [1].

METHODOLOGY

We used the Weather Research and Forecasting (WRF 3.8.1) modeling system for conducting the numerical weather prediction (NWP) experiments to test the hypothesis on the impact of the Brown Ocean effect on the August 2016 Louisiana flooding event [21]. A grid with 3-km spacing over southern Louisiana and centered over the region most impacted by the flood is used in the WRF NWP modeling experiments, with the domain including all of the Gulf coast states and a considerable portion of the Gulf of Mexico. Figure 1b shows the entirety of this 3-km grid, overlaid with 850mb geopotential height and wind barbs. The National Centers for Environmental Prediction (NCEP) Global Forecasting System (GFS) atmospheric analysis and forecast were used to initialize atmospheric conditions in the numerical model grids and also provide time-varying lateral boundary forcing. To initialize land surface conditions, we incorporated output from the NASA Short-term Prediction Research and Transition (SPoRT) Center Land Information System (LIS) assimilating Soil Moisture Active Passive (SMAP) data (Figure 1c). The SPoRT-LIS [22,23] runs the Unified Noah land surface model [24] in an offline mode (i.e., uncoupled to an NWP model), forced by hourly meteorological analyses from the North American Land Data Assimilation System-2 (NLDAS-2) [25] to produce observation-driven soil moisture and temperature analyses over the Continental U.S. at ~3-km grid spacing. Using these best available estimates for soil initial conditions and land surface characteristics, WRF was used to simulate atmospheric evolution for a period of 8 days from 1200 UTC 8 August to 1200 UTC 16 August of 2016. Analysis nudging was applied above the boundary layer for the first 72 hours to establish the

precursor meteorological conditions that led to the development of the tropical depression. Analysis nudging was discontinued after this period to minimize damping of small-scale processes resolved by experiments and the associated internal variability. Optimal model configuration (Table S1) used in the experiments was identified using an ensemble of simulations that considered multiple combinations of initial conditions, lateral boundary forcing and physical parameterizations (Table S2, Figure S3).

We then utilize the above-described simulation as the control and then compare against three sensitivity experiments that consider a combination of soil moisture, and land use and land cover (LULC) change scenarios that modify the potential Brown Ocean effect. These scenarios differ from the control experiments only in the soil moisture initial conditions and land cover classification over southern Louisiana. They are varied (Figure S1) as follows: 1) All wetlands in southern Louisiana are converted to open water; 2) All wetlands are converted to a cropland-natural vegetation mosaic and; 3) Same as scenario (2), except that the initial soil moisture in all the soil layers are reduced by 50%, which is similar to drier antecedent soil moisture conditions in the surrounding regions (Figure 1c; western Louisiana and coastal areas of Mississippi). These LULC change simulations will be referred to herein as open water, cropland wet and cropland dry experiments, respectively.

Note that, the experimental design used in this study is different from prior studies that focused on inland intensification of tropical systems by conducting soil moisture sensitivity analysis [26]. Our experimental design considers variations in surface moisture availability from the perspective of land cover changes occurring in the region and its potential to impact similar events in the future. Analysis of satellite observations between 1985-2010 found wetland loss rate to be ~43 km^2 per year, which is equivalent to losing the area of a football field every hour [27]. The majority of the

conversion is to cultivation, grassland, pasture/hay, developed open space, shrubland, urban development (low, medium and high intensity) and to open water. The cropland vegetation mosaic is chosen as representative of wetland conversion due to anthropogenic activities. Conversion of natural wetlands to anthropogenic land use generally leads to a reduction in moisture availability, both due to changes in surface hydrology and land-atmosphere interactions resulting in rainfall reduction [28]. The cropland wet and cropland dry experiments represent extremes of surface moisture availability that could be expected for the anthropogenic land cover scenario applicable to this region.

Conversion of wetlands to open water is another transition that is important. Land cover change projections suggest transformation of 1300 km^2 of wetlands to open water in coming years as a result of sea-level rise, land subsidence, and development[29]. This type of land cover change will result in a persistent source of surface moisture availability rather than that caused by chance occurrences of antecedent precipitation.

We hypothesize that the high soil moisture conditions (Brown Ocean) resulted in higher storm intensities and thus higher maximum wind speeds and lower minimum pressure. We also postulate that surface characteristics will be influential to the Brown Ocean effect, as they will determine the efficiency of moisture exchange/transport from the land to the atmosphere during storm intensification. The control and cropland wet experiments are scenarios where soil moisture is high, but the efficiency of moisture transport to the atmosphere is expected to vary due to differences in surface characteristics. Compared to the control scenario, the moisture fluxes in the cropland dry scenario are affected due to differences in both soil moisture and surface characteristics. The open water scenario is expected to have features more akin to tropical low-pressure system intensification over the ocean.

RESULTS

Before examining the role of Brown Ocean effect in these NWP experiments, we compared the hourly accumulated rainfall from the control experiment averaged over 2º x 2º region centered on Baton Rouge (all area averages discussed from this point on in the manuscript are for this region) against the corresponding average of National Center for Environmental Prediction (NCEP) hourly Stage IV quantitative precipitation estimates (QPE, Figure 2). Highest observed rainfall rates occurred between 0600 12 August-1800 UTC of 13th of August and this pattern is well captured by the control simulation. However, the initial occurrence of high rainfall rates in the NWP experiments is delayed by ~3 hours compared to the observations. The average accumulated rainfall in the control experiment is 304.65 mm while the observed value was 283.80 mm. Point comparison against rain gauge observations at Baton Rouge also agrees well control experiment (Figure S4).

When compared to spatial patterns of NWS rainfall analysis, control experiments underestimate observed rainfall extremes over parishes to the southwest of Baton Rouge, including the Acadia, Iberia, Vermillion, and Lafayette parishes (Figure 3a and 3b). However, the control experiment captures observed extreme rainfall accumulations in the vicinity of the study area, namely South Baton Rouge and Livingston parishes. The spatial pattern of rainfall accumulations in the control experiment is also consistent with other, prior numerical modeling studies of this event [1]. Thus, there is confidence in the skill of the control simulation to replicate the actual observed weather event. It is worth noting that there are negligible differences in the synoptic features of the simulations; the simulations broadly vary only by the storm strength itself.

To examine the impact of Brown Ocean effect and LULC change on storm structure, we analyzed the time evolution of area-averaged latent heat fluxes at the surface (Figure 4), and minimum geopotential height and maximum wind speed (Figure 5) at 850 hPa level (Figure 5). During day time-hours on the 11th August, the experiments show the most substantial differences in area-averaged latent heat fluxes during the hours when surface insolation is high. This suggests that local buoyancy production of turbulent eddies is the dominant process driving moisture transport during this period. Latent heat fluxes are generally higher for the control, cropland wet and open water experiments compared to cropland dry experiment during the daytime hours of the event. The highest average latent heat fluxes are found in the cropland wet experiment followed by control, open water, and cropland dry experiments.

However, as the storm starts to intensify during the early hours of 12th August (Figure 5), the highest average latent heat fluxes occur in the open water experiment followed by the control, cropland wet and cropland dry experiments. Differences in latent heat fluxes for the entire event time period are statistically significant only for comparisons between open water and other experiments.

The highest maximum wind speed occurs in the open water experiment (31.40 ms^{-1}), followed by the control (27.22 ms^{-1}), cropland dry (24.50 ms^{-1}) and cropland wet (23.41 ms^{-1}) experiments during the intensification stage. The minimum 850 hPa geopotential height is lowest in the control experiment (1464.3 m), followed by the open water (1468.6 m), cropland dry (1478.3 m) and cropland wet (1482.7 m) experiments. Thus, a negative correlation between a minimum of 850 hPa geopotential heights and maximum winds is found only for a subset of the experiments. However, such a pattern is not unusual for small tropical systems [30].

Our experiments show that, as expected, the storm achieves maximum intensity in the open water experiment; and it was interesting to note that storm intensification is adversely affected when the land cover is converted to croplands (Figure 5). Whereas the cropland wet experiment had slightly higher 850 hPa minimum geopotential height and lower maximum wind speeds compared to the cropland dry experiment, higher intensity conditions were maintained in the former scenario for a substantially longer period compared to the latter scenario. Consistent with the Brown Ocean hypothesis, intensification of the storm is clearly impacted by the moisture availability at the surface. However, the Brown Ocean Effect is also shown to be sensitive to the nature of the land cover, as changes in roughness modulate heat, moisture and momentum transfer to the atmosphere. Interactively these changes affect the mesoscale convection, and rainfall resulting from the storm

LULC change scenarios considered in the experiments cause statistically significant differences in average rainfall accumulations over the Baton Rouge area (Figure 2). The time evolution of area-averaged rainfall in all the experiments with high initial surface moisture availability (control, open water, and cropland wet) is similar during the two convective pulse events with high rainfall rates but diverges after the cessation of such events. Compared to the control experiment, the cropland wet and open water experiments resulted in differences in average accumulated rainfall of +3% and -4% respectively, at the end of the analysis period considered. The rainfall evolution in the cropland dry experiment shows substantial differences compared to the other experiments. The rain rates during the two convective pulse events are lower in the cropland dry experiment and lead to a 20% reduction of area-averaged rainfall at the end of the analysis period (Figure 2).

The spatial distribution patterns of rainfall from the storm also show statistically significant differences between the experiments. The main region of enhanced rain (defined here as > 400 mm) in the cropland wet experiment (Figure 3d) is similar to the control scenario (Figure 3b), but

the southern portions are more extensive in the cropland wet experiment. The area of enhanced rainfall in the cropland wet experiment is greater (11,331 km^2) compared to the control experiment (9,342 km^2). Also, the area with accumulated rainfall exceeding 750 mm (most of East Feliciana parish) is also substantially higher in the cropland wet experiment (937 km^2) compared to the control experiment (306 km^2). The region of enhanced precipitation in the open water experiment is reduced (8586 km^2) compared to both control and cropland wet experiments, and the least extent is found in the cropland dry experiment (4,689 km^2). The area where accumulated rainfall exceeds 750 mm is 99 km^2 in the cropland dry experiment, whereas none is present in the open water experiment.

Note that the direct effect of Brown Ocean, which is inland enhancement of latent heat fluxes and convection (Figure S5), is not the only reason for intensification of the storm. Intensification resulting from the direct effect can also indirectly cause additional impact through increase in radial moisture transport from the ocean. We examined the role of this indirect effect by conducting back trajectory analysis for ~1400 locations over the Baton Rouge area, starting at 12 UTC on the 13th of August and extending back for a period of 24 hours. Mean values of air parcel properties and position was computed for the trajectories at regular intervals times (Figures S6 and S7). On average, latent heat fluxes and wind speeds increase as these trajectories approach to land and are substantially higher in the cropland wet and open water experiments, with the enhancement extending some distance inland. Radius-azimuth plots of moisture transport (Figure S8) do indeed show increased southerly transport of moisture in the control, open water, and cropland wet experiments compared to cropland dry experiments. However, there are also substantial contributions to moisture transport from inland regions and directions other than southerly. These

components of moisture transport do respond to changes in land cover and soil moisture and are enhanced in the open water and cropland wet experiments.

Also, changes in surface roughness with land cover also contribute to differences in storm evolution between the experiments[31–33]. Prior study[33], utilizing idealized numerical modeling, examined how intensity and rainfall patterns of landfalling hurricanes respond to variation of moisture availability and surface roughness. In these experiments, rainfall maximums are found on the right side of the approaching storm, with drier land surfaces enhancing this rainfall asymmetry. This is caused by destabilization induced by lower equivalent potential temperature air from land, circulating cyclonically and intruding above surface air on the rear right hand side of the storm. Upon landfall, rainfall maximum switches to the left side of the storm, with frictionally driven convergence of radial component of the storm circulation playing an important role in forcing this feature. On the right hand side of the storm, speed convergence of tangential wind component occur as the offshore flow encounters land surface with higher surface roughness compared to the ocean surface. While convection is also enhanced in this region, advection of rainfall downwind further contributes to rainfall maximum on the left side of the storm. Idealized experiments also examined how landfalling hurricanes respond to changes in surface roughness while keeping the moisture availability constant and vice versa. These experiments found that decay of landfalling hurricanes is more sensitive to an increase in surface roughness than to decrease in the moisture availability. This is attributed to decrease in surface wind speeds caused by higher surface roughness thereby reducing surface latent and sensible heat fluxes.

Even though the nature of storm (near stationary vs. land falling) and experiments conducted (homogenous vs. heterogeneous surface characteristics) is substantially different in the present study, some aspects of the above-described findings from idealized numerical modeling

experiments provide a conceptual basis for analyzing differences found in the LULC experiments. The storm remained relatively stationary during most of its duration, straddling the Louisiana coast. As seen in the idealized experiment for landfalling stage, end members of the current study show that rainfall distribution is most impacted by moisture availability (least in the dry cropland experiments) while surface roughness has the highest impact on storm intensity (open water experiment). In the open water experiment, rainfall on the right side of the storm increases in areas near the coast that are converted to open water (Figure 3e), consistent with rainfall enhancement expected over open water on the onshore flow side of the storm. Rainfall over the open ocean in the offshore flow side of the storm is also enhanced in the dry cropland experiment (Figure 3c, 3d).

Within the four quadrants of a 2^o x 2^o region centered over the storm (Figure S9), we also examined time evolution of average wind speed (Figure S10), wind direction (Figure S11) and rainfall (Figure S12). Maximum differences in the wind speed are found in the lower left and right quadrants. Open water experiment, with least mean roughness in these quadrants, also has the highest wind speeds. Next highest wind speeds in these quadrants are found in cropland wet experiment, which also has the next lowest mean roughness. Control experiment, with the highest mean roughness in the lower left and right quadrants, generally show wind speeds that are smaller compared to both the open water and cropland wet experiment.

During the intensification phase of the storm, maximum differences in rainfall between the experiments occur in the lower right quadrant, with the control and open water experiment having substantially higher rainfall compared to the other experiments. Note that the changes in surface characteristics between the LULC experiments are also maximized in the lower right quadrant (Figure S9). In the open water experiment, enhancement of rainfall results from higher radial

moisture transport resulting from increased flow speeds. However, rainfall in the lower right quadrant is highest in the control experiment, which appears to be caused by enhanced radial transport caused by a directional change in the wind due to higher roughness. In the cropland wet experiment, less radial moisture transport in the lower right quadrant occur during the intensification phase as wind speed is reduced compared to open water experiment and is not compensated by directional changes as in control experiment. Concerning the above discussions, note that changes in moisture transport caused by frictional effects feedback on wind fields through latent heat release and associated alteration of pressure fields. Reduced rainfall in the lower right quadrant in the cropland wet experiment results in high moisture transport to other quadrant and combined with higher wind speeds results in high rainfall in the upper right and left quadrants in this experiment. Differences between the cropland wet and dry experiments suggest that both the reduction in rainfall and storm intensity are driven by diminished moisture availability.

CONCLUSIONS

Synthesis of the numerical modeling results shows that the tropical system that caused the August 2016 extreme Louisiana flooding event is indeed sensitive to the Brown Ocean effect. For scenarios where the total land area was not modified, the existing distribution of wetlands combined with high antecedent soil moisture conditions leads to storm intensification that most closely resembles the intensification pattern expected over oceans. Wetlands to croplands transition resulted in reduction of storm intensity irrespective of soil moisture conditions. Drier conditions also caused 20% reduction in rainfall and shorter durations of high wind conditions. Conversion of wetlands to open water, where the total land area was reduced, resulted in the highest intensity storm. In addition, areal redistribution of rainfall also occurred, reducing rainfall over Baton Rouge while increasing it over areas upwind.

We also found that the modulation Brown Ocean effect by land cover change primarily occurs through process linked to alterations in wind speed and direction. Near surface wind speeds and direction are both affected by surface roughness. Open water experiment has the lowest surface roughness and maximum on-shore wind speed, which along high surface moisture availability and moisture cause the formation of the highest intensity storm. Maximum surface roughness in the coastal regions occurs in the control experiment reduce on-shore wind speeds. However, cross-isobaric flow is enhanced which in combination high moisture availability partially compensate for reduced wind speeds. In the cropland wet experiment, where surface roughness is reduced compared to control experiment while keeping soil moisture constant, increase in on-shore flow is not sufficient to compensate for decreased cross-isobaric flow. This leads to moisture transport further inland and localized increase in rainfall. Differences between the cropland wet and dry simulations shows that, after controlling for surface roughness effects, both storm intensity and rainfall reduce in response to lower moisture availability

Prior studies[26] on the intensification of tropical lows over land found that horizontal moisture transport into the system is approximately equivalent to moisture loss through rainfall. Further, they found that the contribution of surface fluxes of moisture to the total water budget to be small, but important to modulation of convection in the vicinity of the circulation center. The present study suggests that this also applies to the 2016 Louisiana event and drier conditions would have led to reduced storm intensity, substantial reduction of moisture transport within the storm and hence the drastic reduction in accumulated precipitation.

The two major land surface transitions considered in this study, namely conversion of wetlands to cropland mosaic and open water, are reflective of changes that have occurred and continue to occur in southern Louisiana. Our experiments show that, conversion of wetlands to cultivated land will

317 weaken tropical systems such as the one that caused the 2016 Louisiana flood, with the degree of
318 weakening controlled by antecedent soil moisture. On the other hand, conversion of wetlands to
319 open water will lead to intensification of the system and redistribution of rainfall from such events,
320 but persisting in quantities still capable of causing flooding. In other words, the wetland restoration
321 efforts could have broader implications for the region's resiliency.

322 It has been suggested that the probability of tropical system-midlatitude interactions that provided
323 forcing for the mid-August 2016 Louisiana floods[1] has been enhanced due to more frequent
324 propagation of (potentially stronger) upper-level troughs from the western US to the Gulf Coast.
325 Combined with a projected increase in precipitable water due to anthropogenic climate warming,
326 the return time of an event such as the mid-August Louisiana flood event is expected to decrease
327 [34]. Our studies suggest that local LULC change is also of importance. If the current trend
328 continues, LULC change studies in this region indicate that a substantial portion of the wetlands
329 will transition to open water in the coming decades. This will add another ingredient, namely a
330 persistent source of surface moisture availability, i.e., the Brown Ocean Effect will favor
331 recurrence of events such as the 2016 Louisiana floods. Continued LULC transition to open water
332 would likely make the region even more vulnerable to heavy rain events from future tropical
333 systems.

References

1. Wang, S.-Y. S., Zhao, L. & Gillies, R. R. Synoptic and quantitative attributions of the extreme precipitation leading to the August 2016 Louisiana flood. 1–10 (2016). doi:10.1002/2016GL071460

2. Terrell, D. *The Economic Impact of the August 2016 Floods on the State of Louisiana*. (2016).

3. Emanuel, K. The Theory Of Hurricanes. *Annu. Rev. Fluid Mech.* **23,** 179–196 (1991).

4. Pielke Jr., R. A. & Pielke Sr., R. A. *Hurricanes: Their nature and impacts on society*. (John Wiley and Sons, England, 1997).

5. Emanuel, K., Callaghan, J. & Otto, P. A Hypothesis for the Redevelopment of Warm-Core Cyclones over Northern Australia. *Mon. Weather Rev.* **136,** 3863–3872 (2008).

6. Chang, H. I. *et al.* Possible relation between land surface feedback and the post-landfall structure of monsoon depressions. *Geophys. Res. Lett.* **36,** 2–7 (2009).

7. Bozeman, M. L. *et al.* An HWRF-based ensemble assessment of the land surface feedback on the post-landfall intensification of Tropical Storm Fay (2008). *Natural Hazards* **63,** (2012).

8. Andersen, T. K. & Shepherd, J. M. A global spatiotemporal analysis of inland tropical cyclone maintenance or intensification. *Int. J. Climatol.* **34,** 391–402 (2014).

9. Andersen, T. & Shepherd, M. in (eds. Collins, J. M. & Walsh, K.) 117–134 (Springer International Publishing, 2017). doi:10.1007/978-3-319-47594-3_5

10. Kishtawal, C. M., Niyogi, D., Kumar, A., Bozeman, M. L. & Kellner, O. Sensitivity of inland decay of North Atlantic tropical cyclones to soil parameters. *Nat. Hazards* **63,** 1527–1542 (2012).

11. Simpson, R. H. & Pielke, R. A. Hurricane development and movement. *Appl. Mech. Rev.* **29,** (1976).

12. Dastoor, A. & Krishnamurti, T. N. The landfall and structure of a tropical cyclone: The sensitivity of model predictions to soil moisture parameterizations. *Boundary-Layer-Meteorology* **55,** 345–380 (1991).

13. Kellner, O., Niyogi, D., Lei, M. & Kumar, A. The role of anomalous soil moisture on the inland reintensification of Tropical Storm Erin (2007). *Nat. Hazards* **63,** 1573–1600 (2012).

14. Andersen, T. K., Radcliffe, D. E. & Shepherd, J. M. Quantifying surface energy fluxes in the vicinity of inland-tracking tropical cyclones. *J. Appl. Meteorol. Climatol.* **52,** 2797–2808 (2013).

15. Evans, C., Schumacher, R. S. & Galarneau Jr., T. J. Sensitivity in the overland

reintensification of Tropical Cyclone Erin (2007) to near-surface soil moisture characteristics. *Mon. Weather Rev.* **139,** 3848–3870 (2011).

16. Kishtawal, C. M. *et al.* Enhancement of inland penetration of monsoon depressions in the Bay of Bengal due to prestorm ground wetness. *Water Resour. Res.* **49,** 3589–3600 (2013).

17. Xian, Z. A 2-D model study of the influence of the surface on mesoscale convection during the Indian monsoon. Department of Atmospheric Science. (Colorado State University, 1991).

18. McGrath, G. S. *et al.* Tropical cyclones and the ecohydrology of Australia's recent continental-scale drought. *Geophys. Res. Lett.* **39,** 1–6 (2012).

19. Niyogi, D. *et al.* in *Land -Atmospheric Interactions in Asia* (eds. Vadrevu, K. P., Ohara, T. & Justice, C.) (Springer, 2017).

20. Monteverdi, J. P. & Edwards, R. The Redevelopment of a Warm-Core Structure in Erin: A Case of Inland Tropical Storm Formation. *E-Journal Sev. Storms Meteorol.* **5,** 1–18 (2010).

21. Skamarock, W. C. *et al.* A Description of the Advanced Research WRF Version 3. *Tech. Rep.* 113 (2008). doi:10.5065/D6DZ069T

22. Zavodsky, B. T., Case, J. L., Blankenship, C. B., Crosson, W. L. & White, K. D. Application of Next-Generation Satellite Data to a High-Resolution, Real-Time Land Surface Model | Earthzine. *Earthzine* 1–10 (2013).

23. Case, J. L. From drought to flooding in less than a week over South Carolina. *Results Phys.* **6,** 1183–1184 (2016).

24. Ek, M. B. Implementation of Noah land surface model advances in the National Centers for Environmental Prediction operational mesoscale Eta model. *J. Geophys. Res.* **108,** 8851 (2003).

25. Xia, Y. *et al.* Continental-scale water and energy flux analysis and validation for North American Land Data Assimilation System project phase 2 (NLDAS-2): 2. Validation of model-simulated streamflow. *Journal of Geophysical Research* **117,** (2012).

26. Tang, S., Smith, R. K., Montgomery, M. T. & Gu, M. Numerical study of the spin-up of a tropical low over land during the Australian monsoon. *Q. J. R. Meteorol. Soc.* **142,** 2021–2032 (2016).

27. Couvillion, B. R. *et al. Land area change in coastal Louisiana (1932 to 2010).* (2011).

28. Marshall, C. H., Pielke, R. A., Steyaert, L. T. & Willard, D. A. The Impact of Anthropogenic Land-Cover Change on the Florida Peninsula Sea Breezes and Warm Season Sensible Weather. *Mon. Weather Rev.* **132,** 28–52 (2004).

29. Barras, J. *et al.* Historical and Projected Coastal Louisiana Land Changes : 1978-2050.

World **334,** 45 (2004).

30. Callaghan, J. & Smith, R. K. The relationship between maximum surface wind speeds and central pressure in tropical cyclones. *Aust. Meteorol. Mag.* **47,** 191–202 (1998).

31. Tuleya, R. E. Tropical Storm Development and Decay: Sensitivity to Surface Boundary Conditions. *Monthly Weather Review* **122,** 291–304 (1994).

32. Tuleya, R. E., Bender, M. A. & Kurihara, Y. A Simulation Study of the Landfall of Tropical Cyclones. *Monthly Weather Review* **112,** 124–136 (2002).

33. Kimball, S. K. Structure and Evolution of Rainfall in Numerically Simulated Landfalling Hurricanes. *Mon. Weather Rev.* **136,** 3822–3847 (2008).

34. van der Wiel, K. *et al.* Rapid attribution of the August 2016 flood-inducing extreme precipitation in south Louisiana to climate change. *Hydrol. Earth Syst. Sci. Discuss.* **0,** 1–40 (2016).

35. MCST. *MODIS Level 1B Product User's Guide, Version 6.1.14 (Terra)/Version 6.1.17(Aqua)*. (2012).

36. Hunter, J. D. Matplotlib: A 2D Graphics Environment. *Comput. Sci. Eng.* **9,** 90–95 (2007).

Figure Legends

Figure 1. a) True color composite of the tropical disturbance generated using data acquired by Moderate Resolution Imaging Spectroradiometer (MODIS) on the NASA Terra satellite platform[35] (~1630 UTC LST) on 12 August 2016; b) Albedo computed using the 1600 UTC instantaneous shortwave radiation fields in the 3km spacing inner grid in the control experiment. Model simulated cloud fields appear as bright features. Overlaid on the albedo fields are model simulated geopotenital height field (blue) and 850 hPa wind barbs, also valid 12 August 2016; c) NASA SPoRT soil moisture product used to initialize WRF. The red rectangle marks the region of high antecedent soil moisture conditions that potentially modulated the development of the tropical system. Rainfall averaged over this 2^0 x 2^0 rectangular region is used to intercompare the different numerical modeling experiments. Maps were created using Matplotlib, version 1.5.3[36].

Figure 2. Rainfall for the control, cropland dry, cropland wet and open water experiments, averaged over the 2^0 x 2^0 region centered on Baton Rouge (see Figure 1c) are shown using red, yellow, green and blue curves respectively. The purple dashed line shows the NCEP Stage 1V hourly Quantitative Precipitation Estimate averaged over the same region.

Figure 3. Spatial distribution of accumulated rainfall from: a) Observations; b) Control experiment; c) Cropland dry experiment; d) Cropland wet experiment and; e) Open water experiment. Maps were created using Matplotlib, version 1.5.3[36].

Figure 4. Surface latent heat fluxes for the control, cropland dry, cropland wet and open water experiments, averaged over the 2^0 x 2^0 region centered on Baton Rouge (see Figure 1c) are shown using blue, green, red and aqua curves respectively.

Figure 5. Time evolution of maximum wind speed (dashed) and minimum geopotential height at 850 hPa for the different experiments.

Acknowledgments

Udaysankar Nair and Emily Foshee are supported under NSF CAREER grant AGS-1352046. D. Niyogi acknowledges support from NSF CAREER grant AGS-0847472, NSF Extreme Rain AGS-1522494, NSF RAPID AGS-1902642, and USDA Hatch grant. W. Smith is supported under grants NSF AGS 1445875 and NSF AGS 1415244. M. Shepherd acknowledges support from NASA Grant NNX11AL86H. R. Pielke Sr. acknowledges support from NSF AGS grant 1552487. The authors thank Dr. Barry Keim, State Climatologist for Louisiana for technical assistance. The manuscript benefited from discussions with Dr. Melville Nicholls. The Terra MODIS Level-1B data was acquired from the Level-1 and Atmosphere Archive & Distribution System (LAADS) Distributed Active Archive Center (DAAC) housed at the Goddard Space Flight Center in Greenbelt, Maryland (https://ladsweb.nascom.nasa.gov/). The subsetting, mosaicking and reprojection services offered through the LAADS ordering system were utilized to pre-process the MODIS Level-1B data.

Author Contribution

R. A. Pielke Sr. proposed investigating the role of land-atmosphere interactions in development of

the tropical system that caused the 2016 Louisiana flood. E. Rappin led the design of numerical model experiments with contributions from U. Nair, R. A. Pielke, R. Mahmood, J. Santanello and D. Niyogi. M. Shepherd suggested some of the rainfall analysis methods. D. Niyogi and M. Shepherd provided context on the concept of the "Brown Ocean Effect". J. Case and C. Blankenship assisted in the utilization of SPoRT soil moisture data products. U. Nair, E. Rappin, E. Foshee, W. Smith, and J. Case analyzed model output assisted by the other authors. All the authors contributed to the authoring of the manuscript.

Additional Information

Supplementary information is provided along with the manuscript.

Competing Financial Interests

The authors declare that there are no competing interests.

Materials and Correspondence

Correspondence and request for material should be addressed to U. Nair.

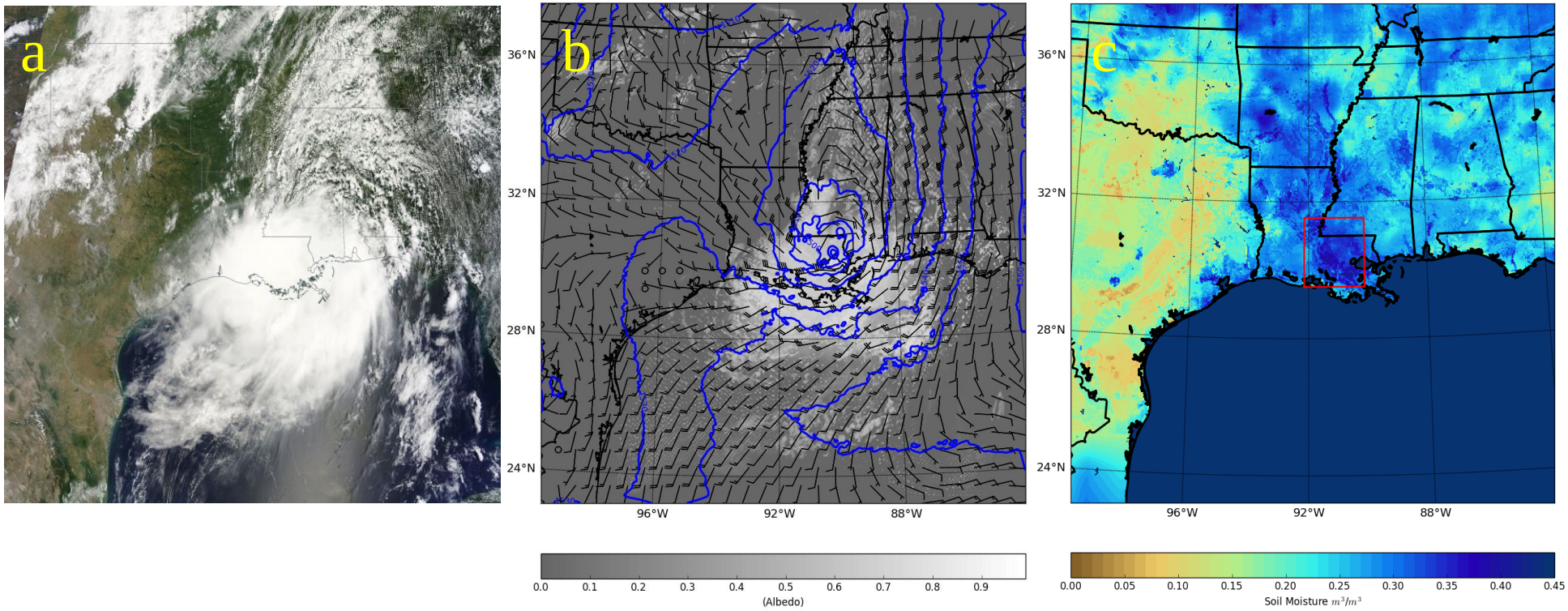
a
b
c
36°N
32°N
28°N
24°N
96°W
92°W
88°W
0.0 0.1 0.2 0.3 0.4 0.5 0.6 0.7 0.8 0.9
(Albedo)
0.00 0.05 0.10 0.15 0.20 0.25 0.30 0.35 0.40 0.45
Soil Moisture m^3/m^3

Figure 1

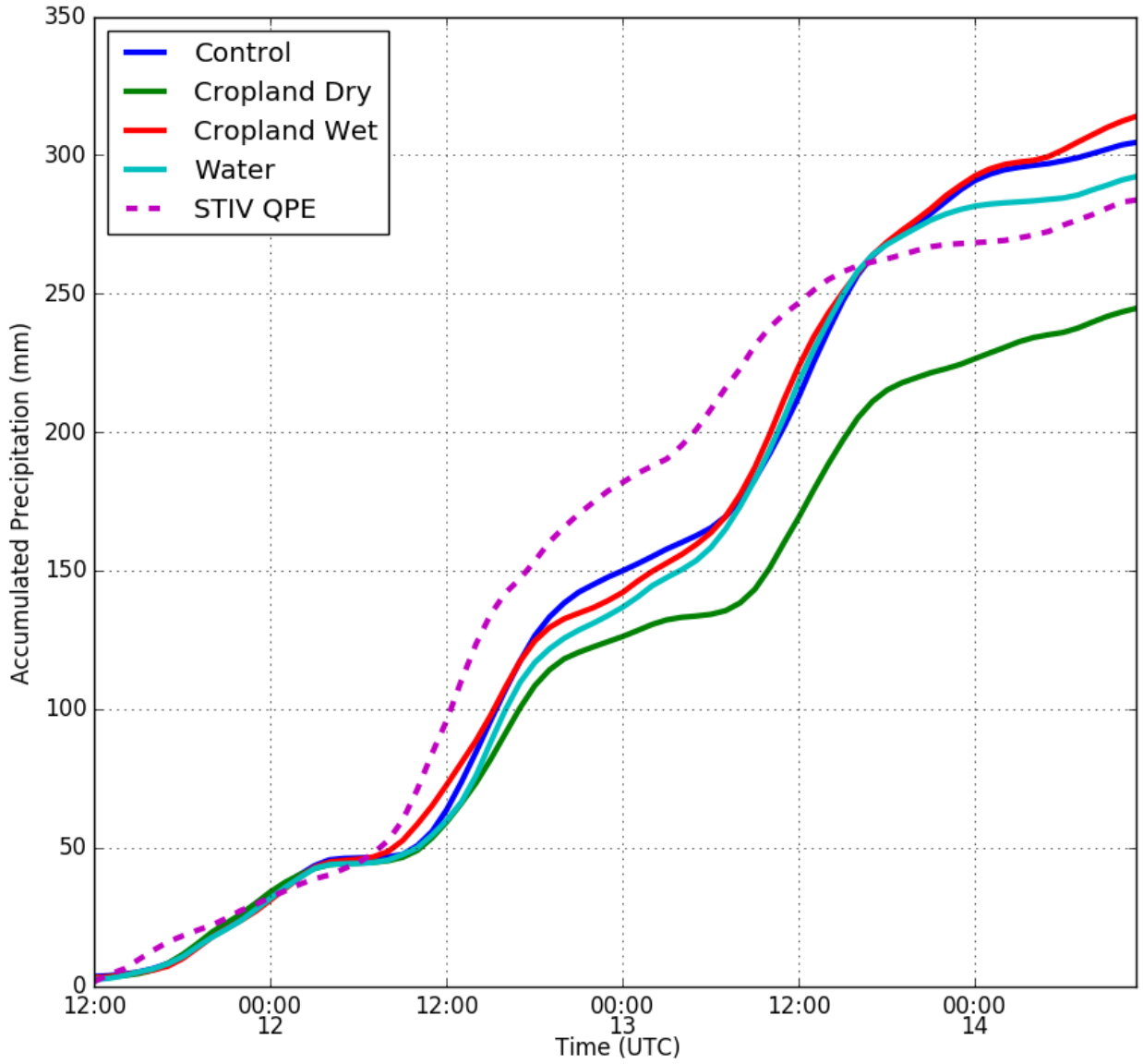
Control
Cropland Dry
Cropland Wet
Water
STIV QPE
Accumulated Precipitation (mm)
0
50
100
150
200
250
300
350
12:00
00:00
12
12:00
00:00
13
12:00
00:00
14
Time (UTC)

Figure 2

.

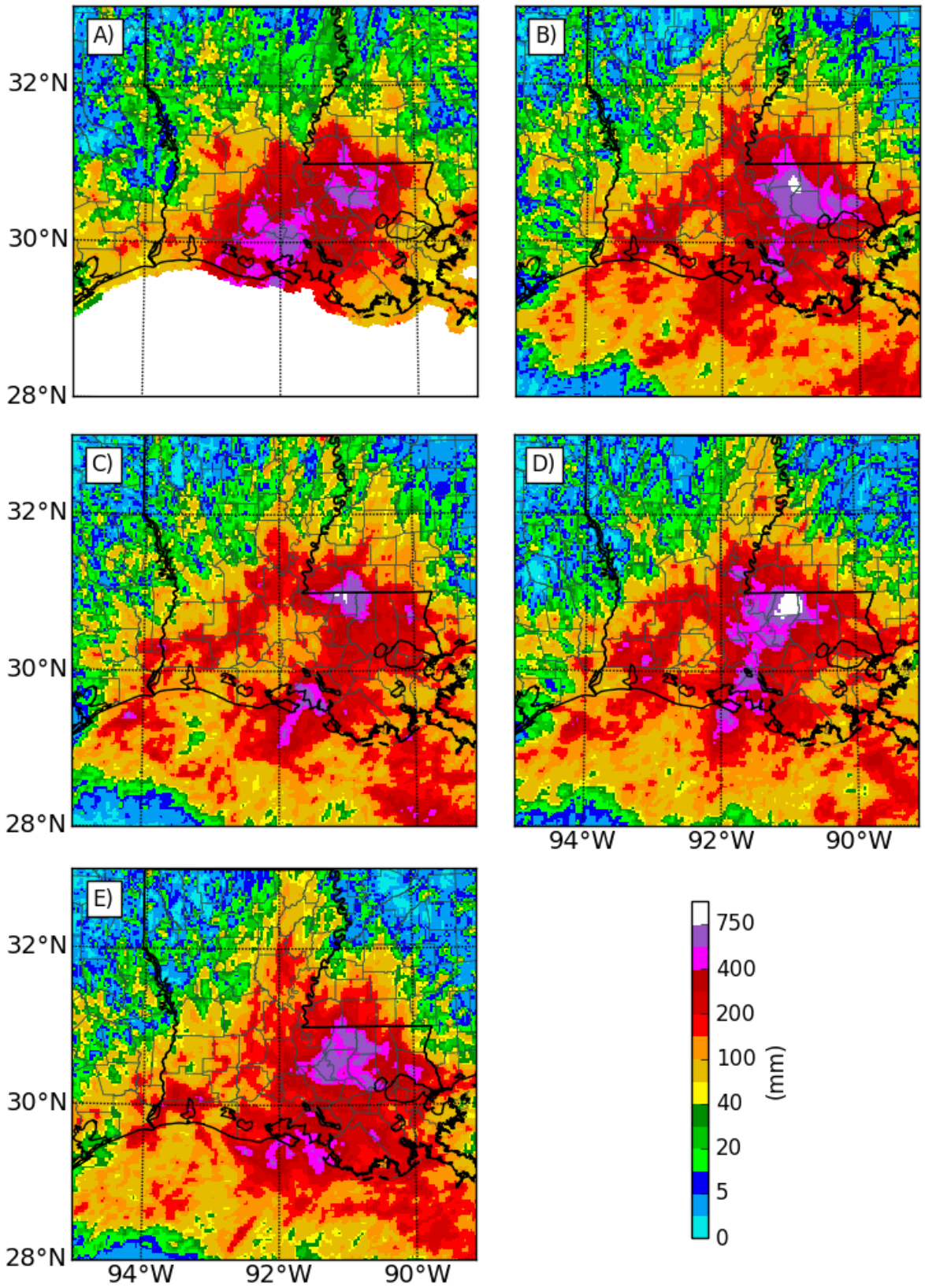

Figure 3

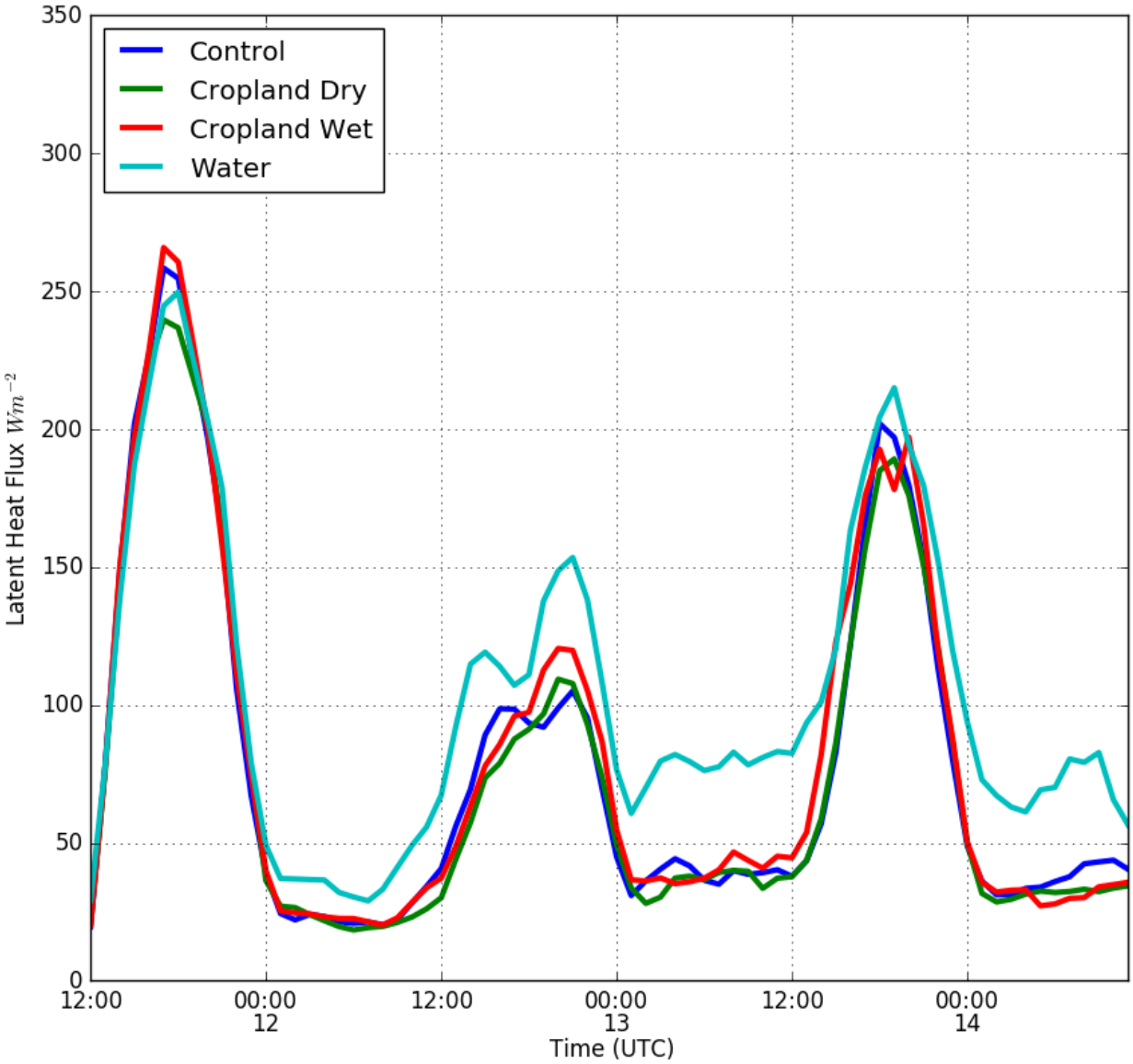
Control
Cropland Dry
Cropland Wet
Water
Latent Heat Flux Wm^{-2}
350
300
250
200
150
100
50
0
12:00
00:00
12
12:00
00:00
13
12:00
00:00
14
Time (UTC)

Figure 4

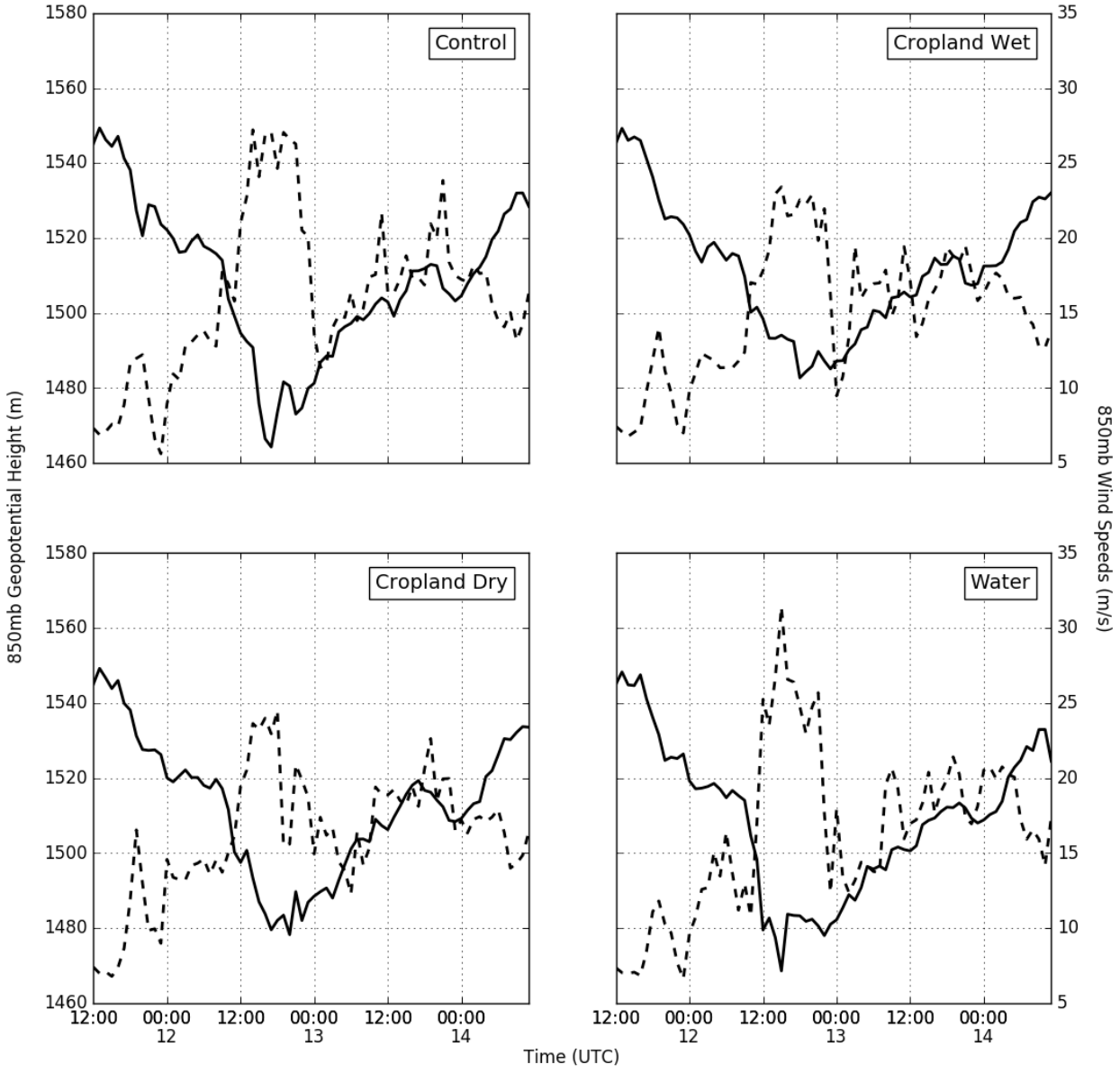
Control
Cropland Wet
Cropland Dry
Water
850mb Geopotential Height (m)
850mb Wind Speeds (m/s)
Time (UTC)
1580
1560
1540
1520
1500
1480
1460
35
30
25
20
15
10
5
12:00
00:00
12
13
14

Figure 5

Supplementary material

Influence of Land Cover and Soil Moisture based Brown Ocean Effect on an Extreme Rainfall Event from a Louisiana Gulf Coast Tropical System

Udaysankar S. Nair[1], Eric Rappin[2], Emily Foshee[1], Warren Smith[3,4], Roger A. Pielke Sr.[4], Rezaul Mahmood[5], Jonathan L. Case[6], Clay B. Blankenship[7], Marshall Shepherd[8], Joseph A. Santanello[9], Dev Niyogi[10]

[1]Department of Atmospheric Science, University of Alabama in Huntsville, Huntsville, AL 35806

[2] Department of Geography and Geology and Kentucky Climate Center, Western Kentucky University, Bowling Green, KY 42101

[3]Department of Atmospheric and Oceanic Sciences, University of Colorado Boulder, Boulder, CO 80309

[4]Cooperative Institute for Research in Environmental Sciences, University of Colorado Boulder, Boulder, CO 80309

[5]High Plains Regional Climate Center, School of Natural Resources, University of Nebraska-Lincoln, Lincoln, NE 68583

[6]ENSCO, Inc./NASA Short-term Prediction Research and Transition (SPoRT) Center

[7] Universities Space Research Association, NASA Short-term Prediction Research and Transition (SPoRT) Center

[8]University of Georgia, Department of Geography, Atmospheric Sciences Program

[9]NASA-GSFC, Hydrological Sciences Laboratory, Greenbelt, MD

[10]Department of Agronomy and Department of Earth, Atmospheric and Planetary Sciences, Purdue University, West Lafayette, IN 47907, USA

WRF Configuration: The Weather Research and Forecast (WRF) model is a regional, non-hydrostatic numerical model developed by the National Center for Atmospheric Research [20]. WRF solves governing equations of atmospheric flow utilizing finite difference formulations on an Arakawa C-Grid in the horizontal and a terrain following sigma-p coordinates in the vertical. A variety of parameterization schemes are available for representing physical processes, the details of which are provided in *Skamarock et al.* [2008].

In this study, the Advanced Research WRF model version 3.8.1 was configured using a single domain with a 3 kilometer grid spacing in both the x and y directions centered at 30.5^0N, 92^0W. A total of 560x560 horizontal mass points and 61 vertical levels are utilized with 15 lowest vertical levels being located within the planetary boundary layer. Details of the physical parameterizations and other relevant model configuration variables are provided in Table 1.

The Short Term Prediction and Research Transition Center's (SPoRT) Real-Time Land Information System (LIS) provides high resolution land surface initial conditions for weather prediction models at real time. The SPoRT LIS domain of 3km grid spacing covers most of the central and eastern United States and ingests NASA MODIS satellite derived Greenness Vegetation Fraction and thus provides observational constraints on vegetation phenology. The land cover classification in WRF is specified using the MODIS land cover dataset (Figure S1).

Domain	
Number of Domains	1
Grid Spacing (dx & dy)	3 km
Start Date	August 8, 2016 12Z
End Date	August 16, 2016 12Z
Input Data	FNL & SpoRT-LIS land surface conditions

Center Latitude/Longitude	30.5degN, 92.0degW
Input Data Interval	6 hours
Number of Vertical Levels	61
Number of Vertical Levels in Lowest 1 km	15
Time Step	15 seconds
Radiation Time Step	5 minutes
Top Pressure Level	5000 Pa
Number of Soil Layers	4
Static Geographic Data Resolution	15 seconds
Parameterization Schemes	
Microphysics	Thompson aerosol-aware (option 8)
Radiation (Shortwave)	RRTMG (option 4)
Radiation (Longwave)	RRTMG (option 4)
Planetary Boundary Layer	Mellor-Yamada-Janjic (option 2)
Cumulus	None
Surface Layer	Monin-Obukhov (Janjic, option 2)
Land/Water Surface	Noah Land Surface Model (option 2)
Urban	None
Dynamics	
Turbulence/Mixing	W-Rayleigh (Relaxation, option 3)
Diffusion	2nd Order (option 1)

Table S1: WRF options used in each of the discussed simulations

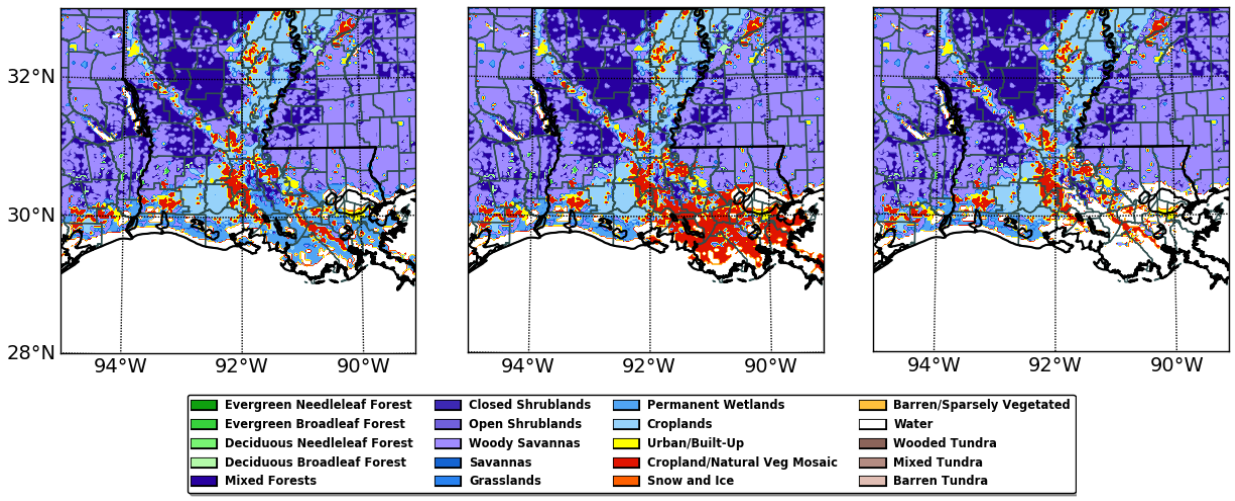

Figure S1. Land cover map applicable to control, cropland wet, cropland dry and open water experiment are show in the top left, top right, bottom left and bottom right panels, respectively. Maps were created using Matplotlib, version 1.5.3 (https://matplotlib.org/1.5.3/contents.html).

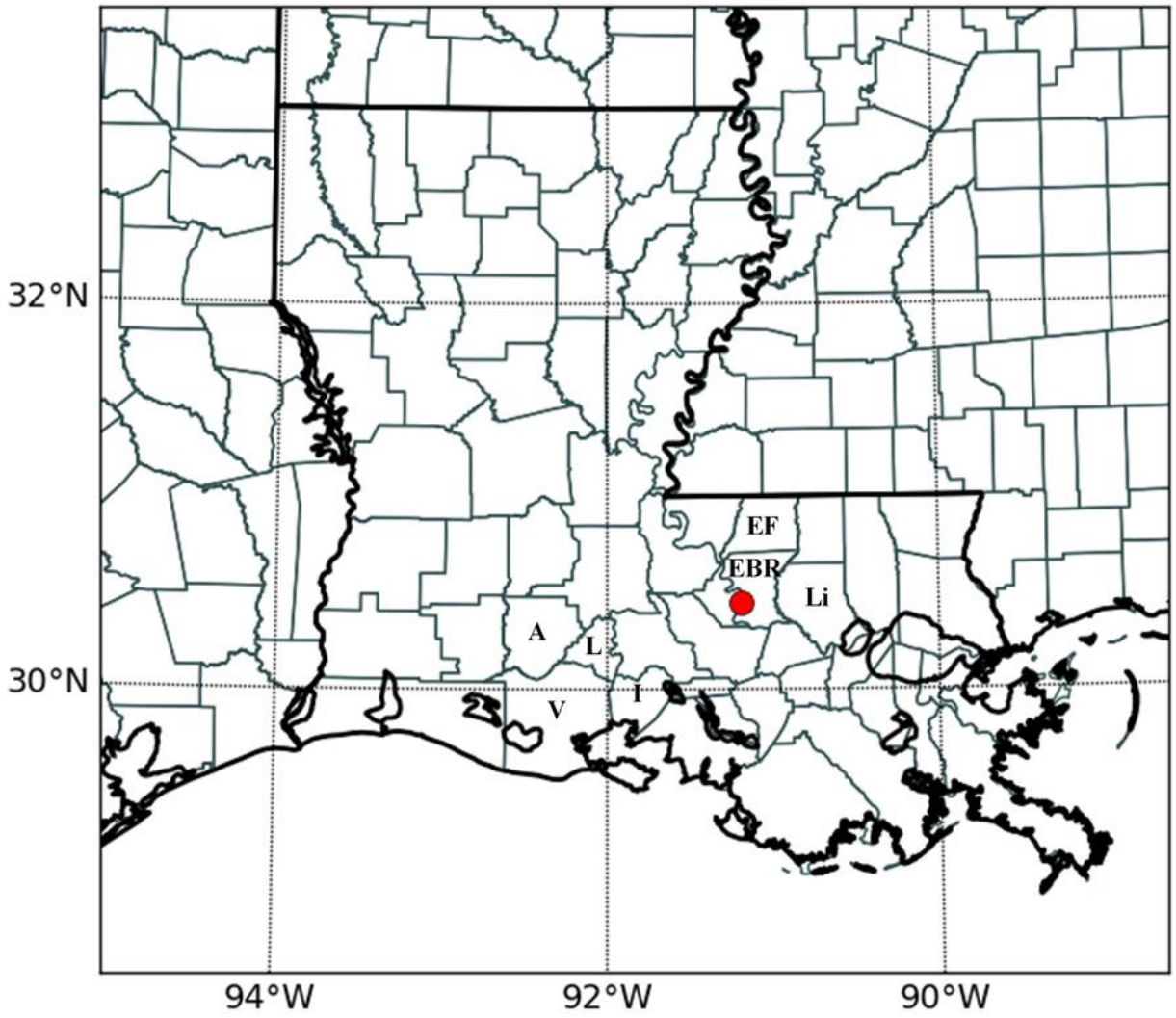

Figure S2. Locations of the East Feliciana, East Baton Rouge, Livingston, Acadia, Lafayette, Iberia and Vermilion parishes are marked as EF, EBR, Li, A, L, I and V respectively. Maps were created using Matplotlib, version 1.5.3 (https://matplotlib.org/1.5.3/contents.html)

Selection of model parameterization and initial/boundary conditions. An ensemble of simulations was conducted (Table S2) to determine which suite of physical parameterizations and initial/boundary conditions accurately reproduced the magnitude and geographical distribution of precipitation of the flood event. As the lower boundary initial condition was generated with the Noah Land Surface Model, that parameterization was not changed. The table below provides information on.

Experiment	Lateral Forcing	Surface Forcing	Microphysics	PBL physics
Control	FNL	LIS SMAPDA	Thompson	MYJ
1	FNL	LIS	Thompson	MYJ
2	NAM	LIS SMAPDA	Thompson	MYJ
3	NAM	LIS	Thompson	MYJ
4	FNL	LIS SMAPDA	WSM6	MYJ
5	FNL	LIS SMAPDA	Thompson	YSU
6	FNL	LIS SMAPDA	Thompson	MYNN2

Table S2. different initial/boundary conditions and parameterizations considered in the ensemble of simulations. FNL: NCEP Final Global Analysis; NAM: 12 km North American Mesoscale Forecast System Analysis; LIS: NASA SPORT 3km Land Information System; LIS SMAPDA: NASA SPORT 3km LIS with SMAP Data Assimilation; Thompson: Thompson microphysics – double moment for ice and rain; WSM6: WRF single moment six class microphysics; MYJ: Mellor – Yamada – Janjic PBL scheme; YSU: Yonsei University PBL scheme; MYNN2: Mellor – Yamada – Nakanishi – Niino level 2.5 PBL scheme.

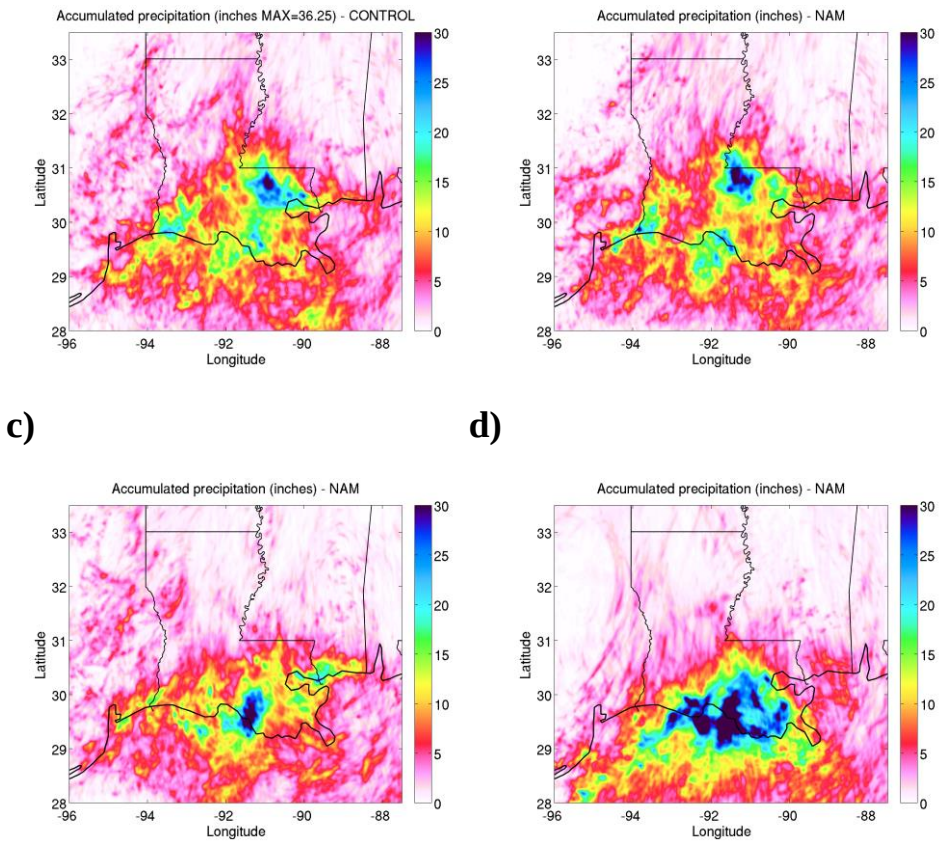

Physics and forcing ensemble performed: a) Control, b) Exp. 1, c) Exp. 2, d) Exp. 6.

Figure S3. Spatial patterns of accumulated precipitation (inches) from: a) Control; b) Exp 1, c) Exp 2; d) Exp 3. Maps were created using Matlab R2017a (https://www.mathworks.com/products/new_products/release2017a.html)

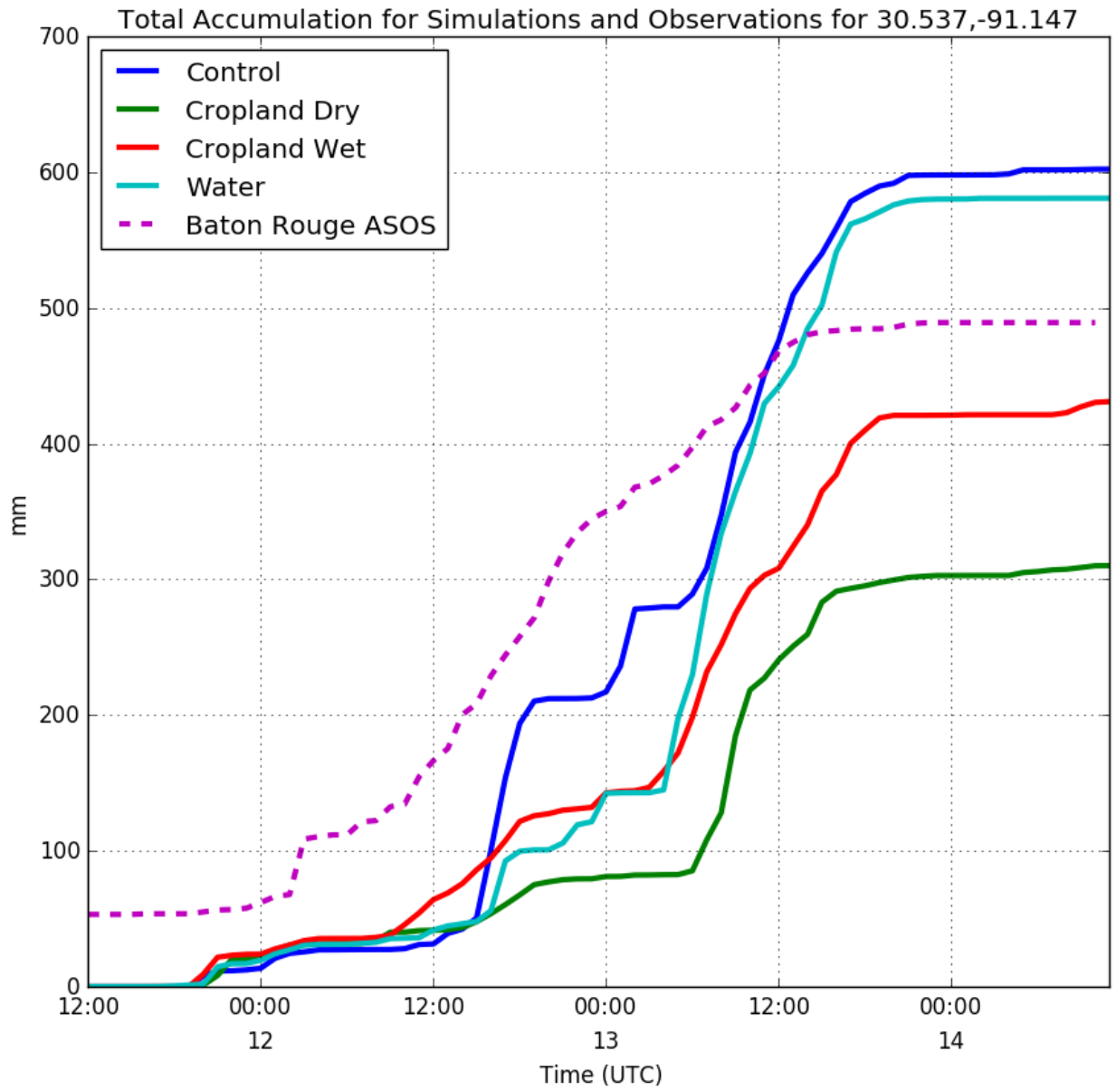

106

107 Figure **S4**. Model simulated rainfall at the ASOS location showing a wide range of variability in
108 response to soil moisture and LULC changes (Figure 2). All the LULC change scenarios
109 considered led to local reduction in rainfall at the ASOS observation location. Compared to the
110 control simulation, the open water, cropland dry and cropland wet LULC change scenarios
111 resulted in local rainfall changes of -3%, -26% and -48%, respectively.

112

Analysis of Latent Heating: Vertical profiles of latent heating for the experiments also show differences among the experiments (Figure S5). Prior to the intensification of the system, substantial differences in the vertical profile of latent heating is found, with the cropland wet experiment showing up to 50% more latent heating compared to other experiments. Note the initial decline in 850hPa geopotential height is highest for the cropland wet experiment.

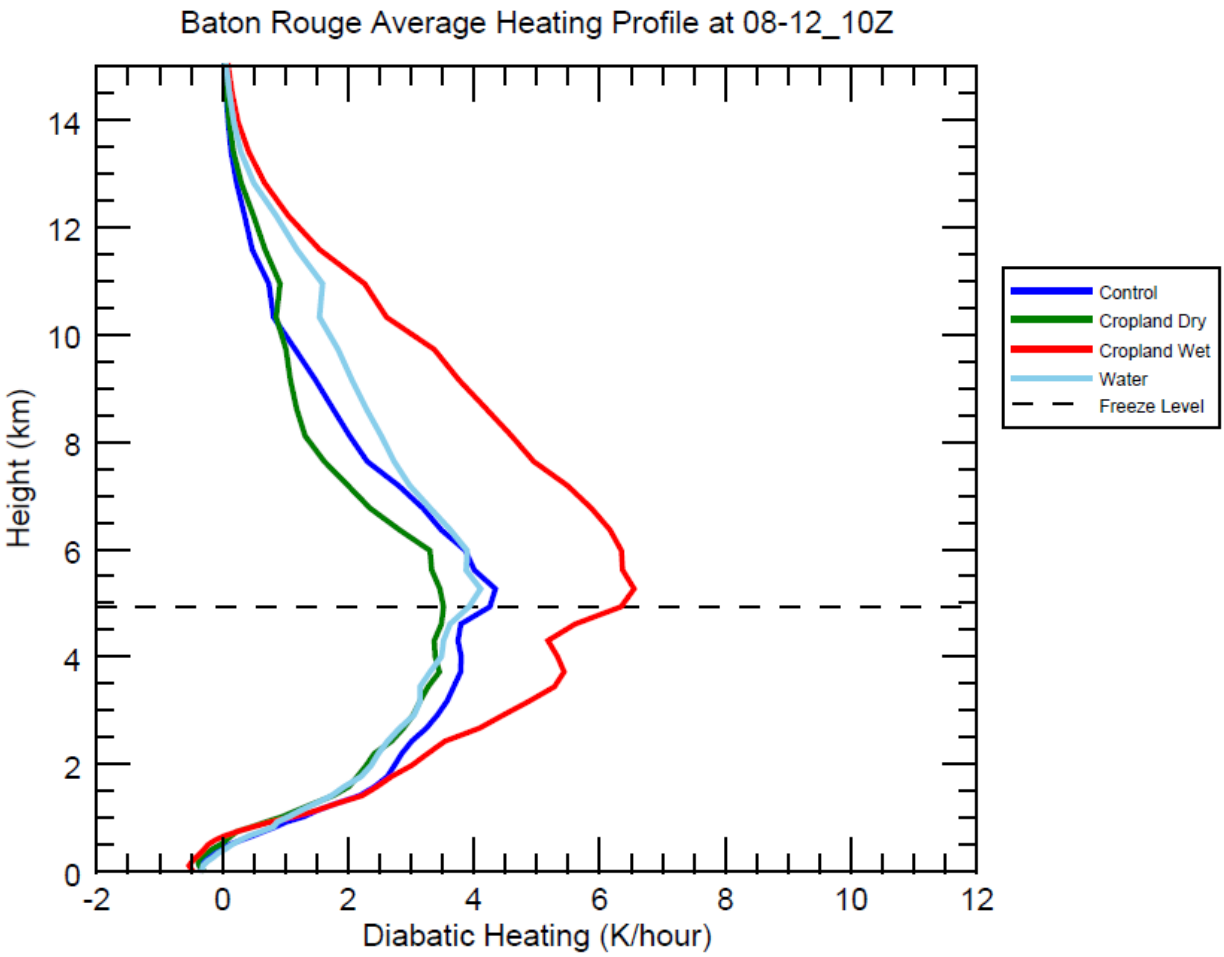

Figure S5. Area averaged vertical profiles of latent heat release at 1000 UTC on August 12 for the different experiments.

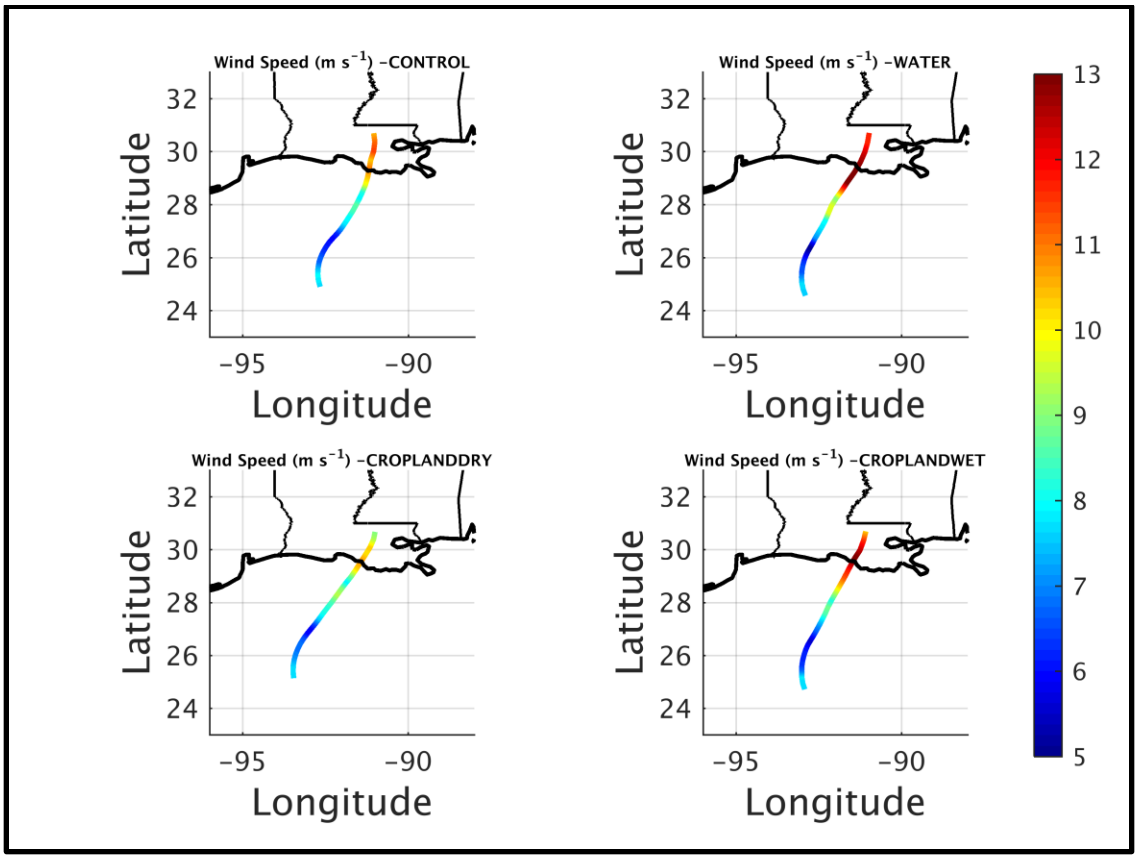

122

123 **Figure S6**. Mean values of wind speed along the mean position of 24 hour back trajectory
124 intiated from points over Baton Rouge for control, open water, cronpland dry and cropland wet
125 experiments. Maps were created using Matlab R2017a (
126 https://www.mathworks.com/products/new_products/release2017a.html).

127

128

129

130

131

132

133

134

135

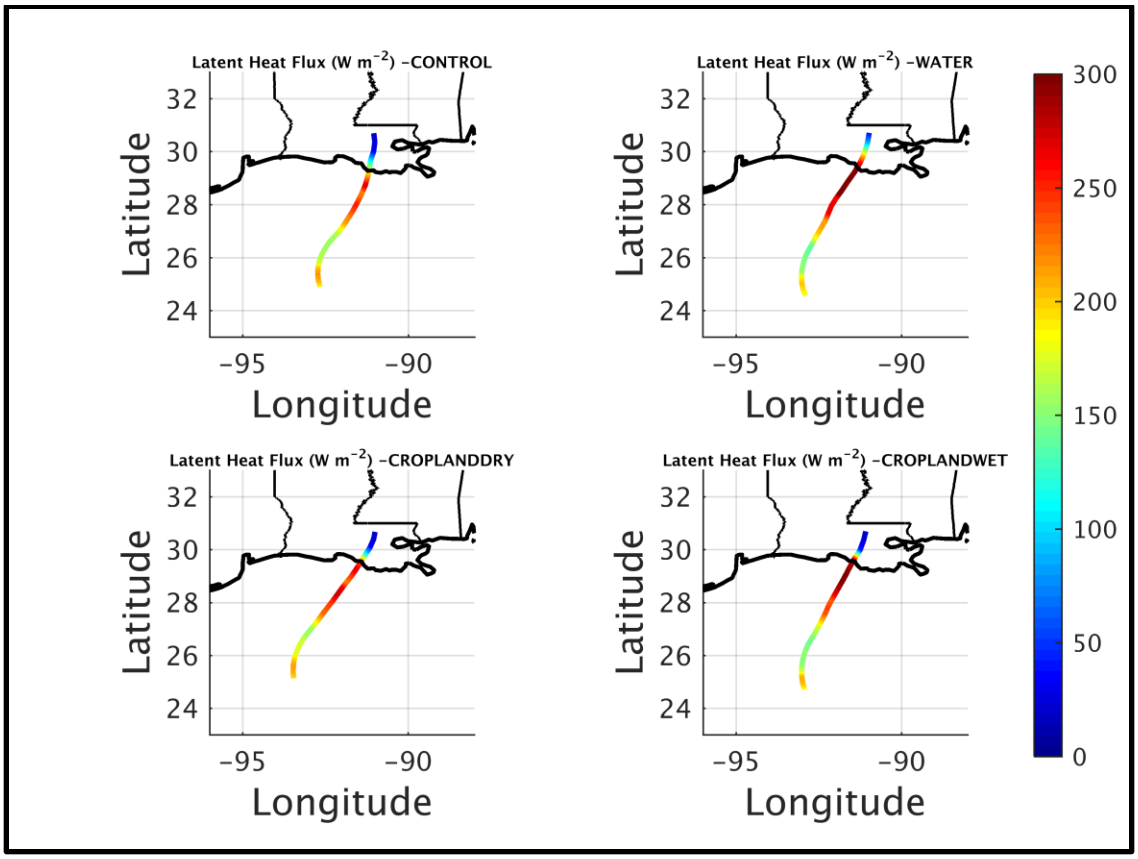

Figure S7. Mean values of latent heat fluxes along the mean position of 24 hour back trajectory intiated from points over Baton Rouge for control, open water, cronpland dry and cropland wet experiments. Maps were created using Matlab R2017a (https://www.mathworks.com/products/new_products/release2017a.html).

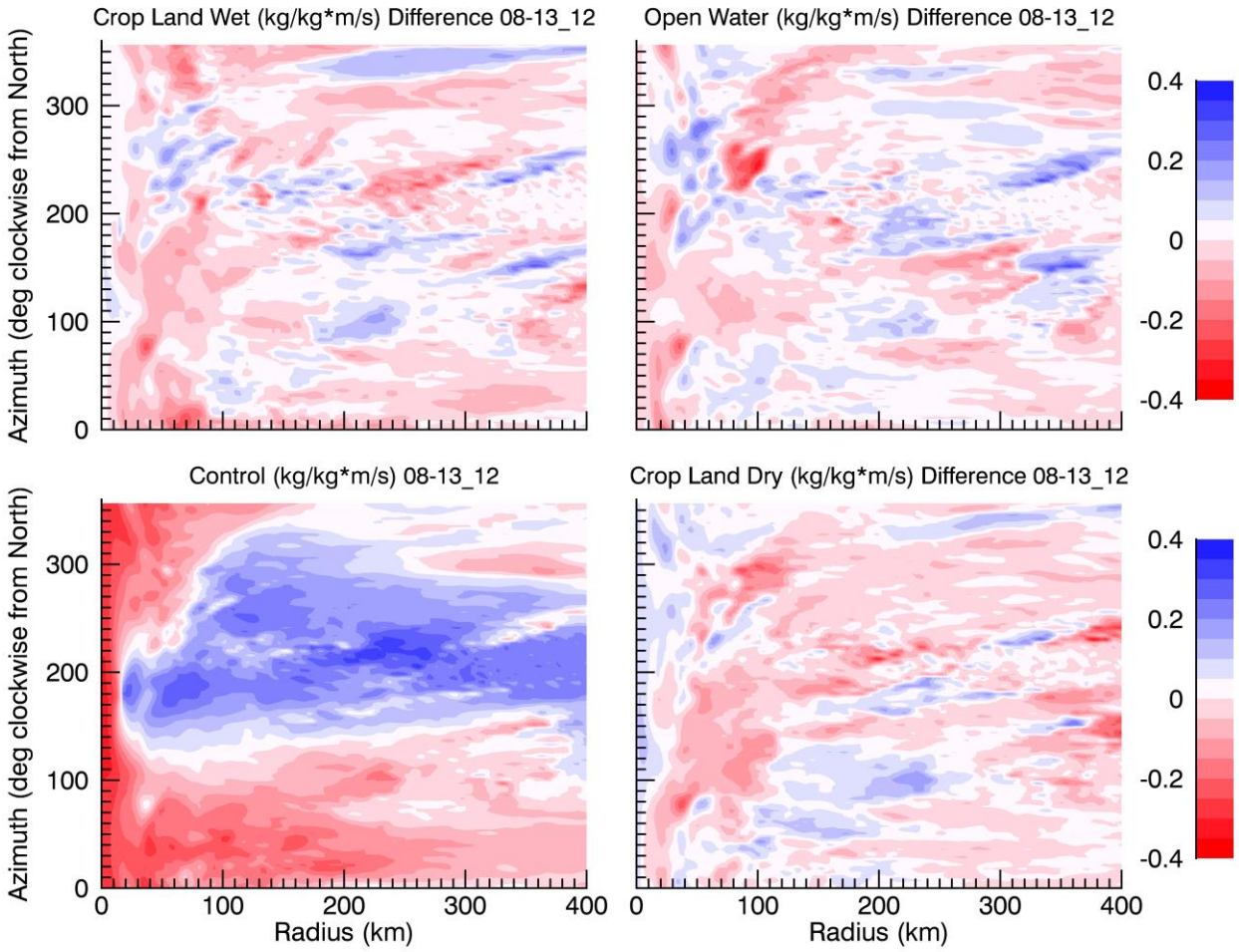

Figure S8. Radius-azimuth plot of moisture transport for cropland wet, open water, control and cropland dry experiments..

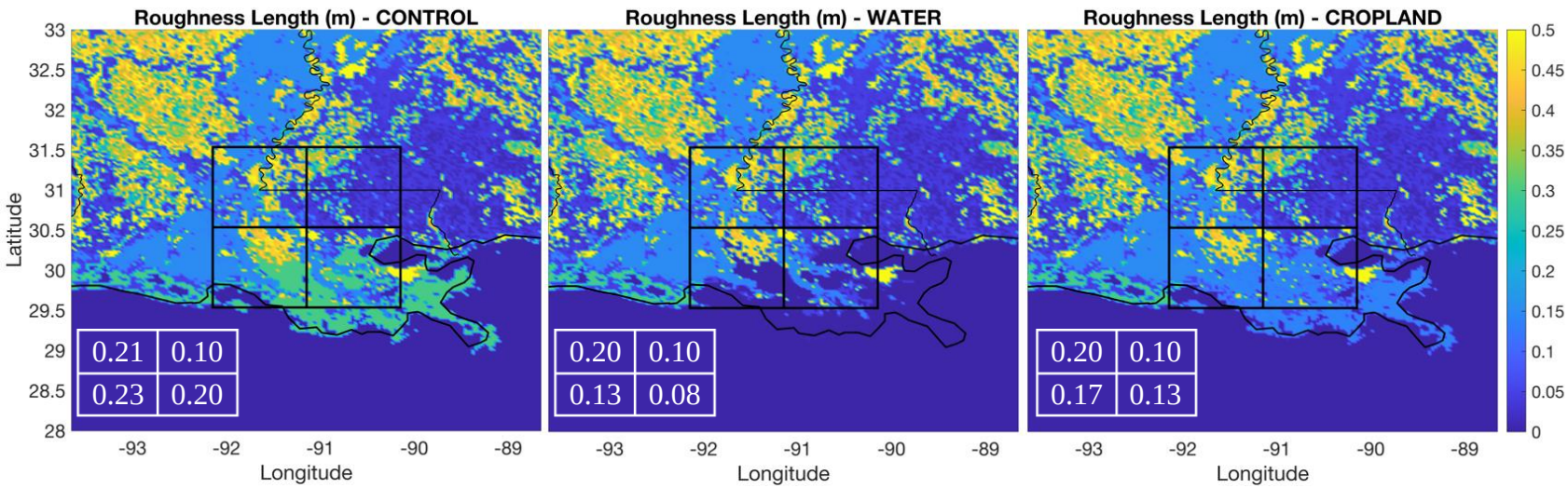

Figure S9. Spatial distribution of surface roughness used in the different experiments. Left, middle and right panels are for control, open water and cropland (wet/dry) experiments respectively. The four quadrants used for analysis described in the text are outlined in black. The tables in the inset of each panel shows the average roughness length in each of the quadrant. Maps were created using Matlab R2017a (https://www.mathworks.com/products/new_products/release2017a.html).

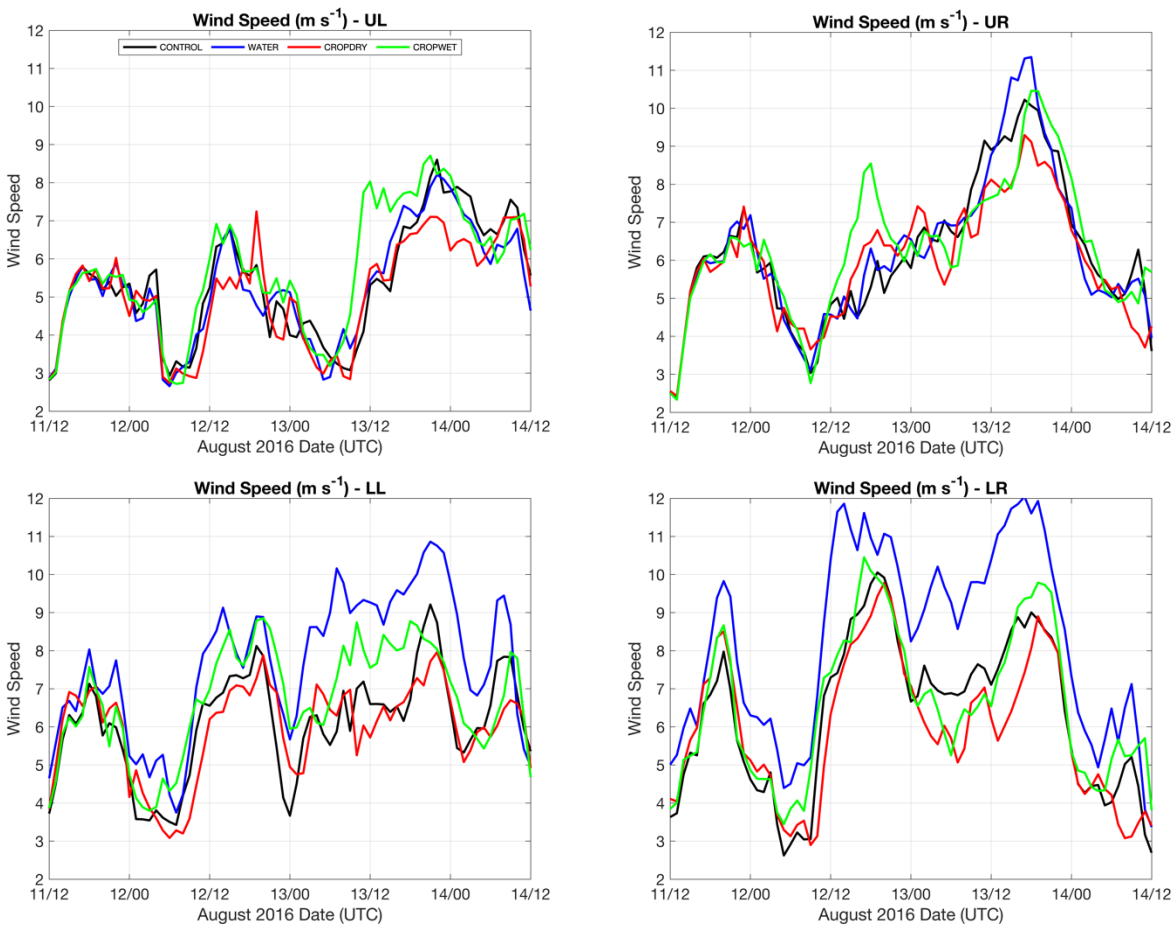

Figure S10. Time evolution of average surface wind speeds in each of the analysis quadrants shown in Figure S9.

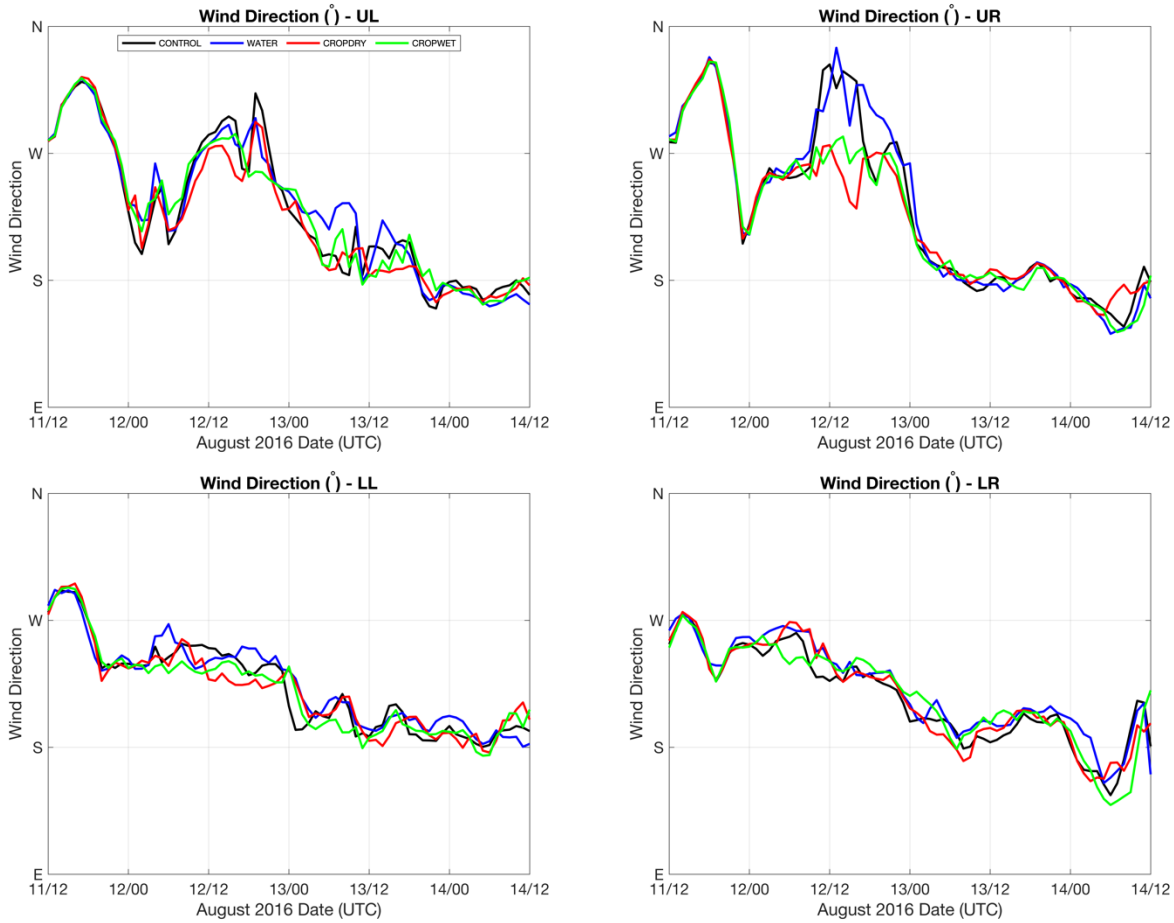

Figure S11. Time evolution of average surface wind direction in each of the analysis quadrants shown in Figure S9.

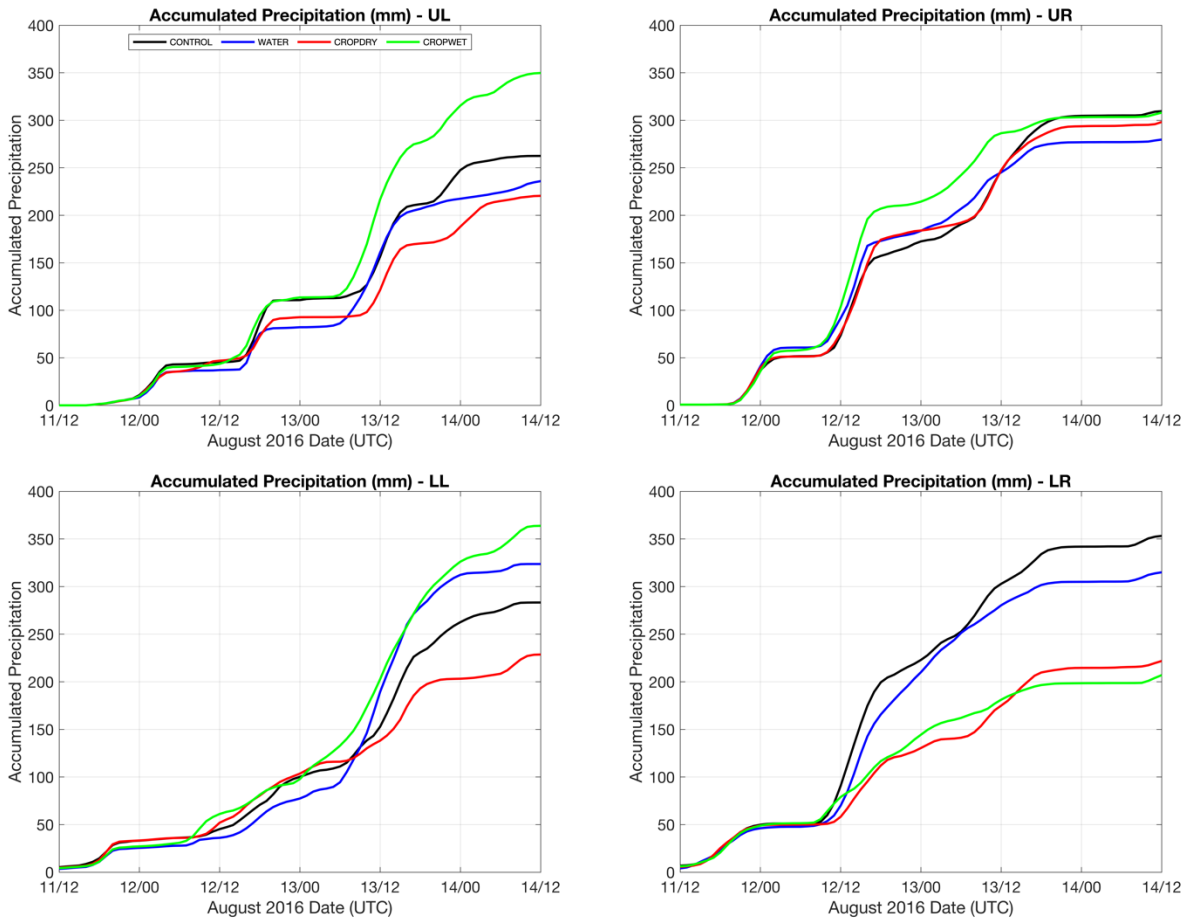

Figure S11. Time evolution of average surface rainfall accumulation in each of the analysis quadrants shown in Figure S9.

253

254

255

256

257

258

259

260

261